

Urban Region Pre-training and Prompting: A Graph-based Approach

Jiahui Jin¹, Yifan Song¹, Dong Kan¹, Haojia Zhu¹, Xiangguo Sun², Zhicheng Li¹, Xigang Sun¹,
Jinghui Zhang¹
¹Southeast University
²The Chinese University of Hong Kong

Abstract

Urban region representation is crucial for various urban downstream tasks. However, despite the proliferation of methods and their success, acquiring general urban region knowledge and adapting to different tasks remains challenging. Previous work often neglects the spatial structures and functional layouts between entities, limiting their ability to capture transferable knowledge across regions. Further, these methods struggle to adapt effectively to specific downstream tasks, as they do not adequately address the unique features and relationships required for different downstream tasks. In this paper, we propose a **Graph-based Urban Region Pre-training and Prompting framework (GURPP)** for region representation learning. Specifically, we first construct an urban region graph that integrates detailed spatial entity data for more effective urban region representation. Then, we develop a subgraph-centric urban region pre-training model to capture the heterogeneous and transferable patterns of interactions among entities. To further enhance the adaptability of these embeddings to different tasks, we design two graph-based prompting methods to incorporate explicit/hidden task knowledge. Extensive experiments on various urban region prediction tasks and different cities demonstrate the superior performance of our GURPP framework.

Keywords

Urban Computing, Urban Region Representation Learning

1 Introduction

An urban region is a geographical area comprising diverse spatial entities (e.g., shopping centers, restaurants, and roads) and their interactions (e.g., nearby and located in). Recently, urban region representation learning, which aims to extract vector embeddings from these entities, has become a significant research focus [60]. Effective urban region representations can be applied to various tasks, such as region popularity prediction [10, 24, 46, 65], house price prediction [45], crime prediction [45, 46, 59, 65], and population density inference [23], enabling urban planners, policymakers, and businesses to enhance decision-making processes. However, the complexity of urban environments and the diversity of applications pose significant challenges.

Balancing urban generality and task specificity is crucial in urban region representation. **(i) Urban regions often appear similar in their spatial structures and functional layouts**, because the interactions among entities within these regions follow similar patterns. These shared patterns serve as generic knowledge across urban areas, facilitating the development of generalizable region representation models. As illustrated in Figure 1, Region A and

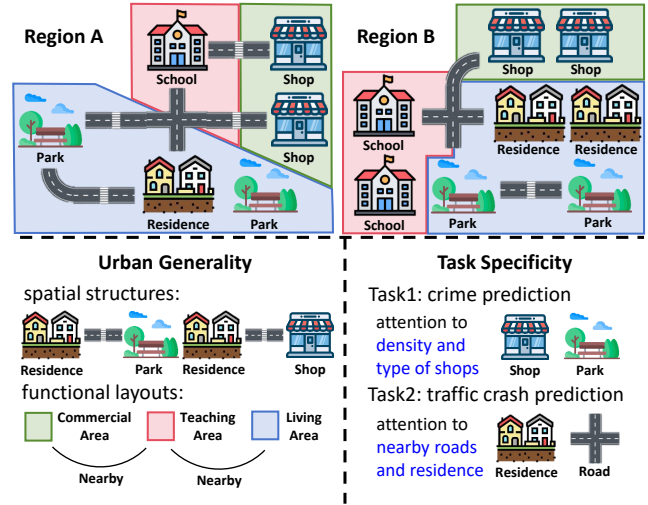


Figure 1: Example of urban generality and task specificity.

Region B showcase typical urban regions. In these examples, spatial structures are demonstrated by the proximity of residences to parks and shops, which enhances community convenience and accessibility. Functional layouts are characterized by the clustering of similar entities within areas, such as shops in commercial areas and schools in teaching areas, and the close proximity of these distinct areas to each other. Therefore, an effective urban region representation model needs to capture the heterogeneous and generic patterns of interactions among entities within regions. **(ii) Despite the broad similarities, each urban region and downstream task possesses unique details.** Specific tasks may require attention to different features within urban data. For example, in traffic crash prediction, the density of roads and the number of residents living nearby, might be critical features, as they directly influence the probability of accidents occurring. On the other hand, crime prediction models might focus on the density and type of POIs within the region, such as bars or late-night convenience stores. As consequence, balance between generality and specificity raises a crucial question: Can we design an urban region representation framework that effectively integrates generalizable knowledge while accommodating the specific needs of distinct tasks?

Recently, the pre-training and prompting paradigm that learns general representations that can be fine-tuned or prompted to adapt to specific tasks has shown remarkable success in the field of natural language processing [4, 11, 27, 39] and computer vision [38, 63, 64]. Inspired by these advancements, we hope to design a pre-training and prompting framework for urban region representation learning.

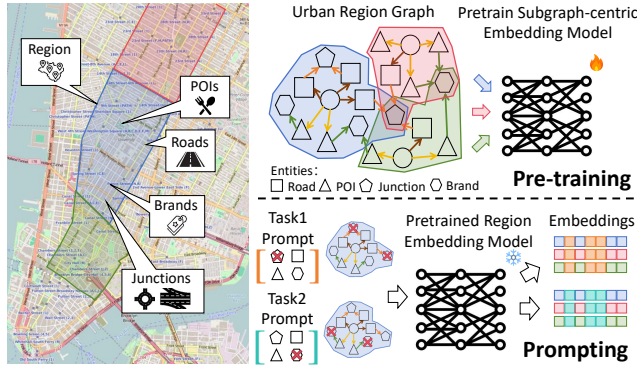


Figure 2: Main idea of urban pre-training and prompting

However, building such a framework for urban representation is never easy. The challenges are as follows.

(1) Capturing the heterogeneous and generic patterns of interactions among spatial entities within regions is hard. Most previous methods follow a process where they first predefine aggregations and statistics about urban entities and relationships, and then learn from these predefined features [13, 23, 50, 58]. While this approach has its merits, it often fails to capture the spatial structures and functional layouts between entities within regions which is generalizable. Other previous methods consider urban entities in isolation, but they focus on only a few types, such as POIs and roads and a few relations between them. This narrow focus limits their ability to capture the heterogeneous and generic patterns of interactions among entities, resulting in embeddings that are less robust and less effective [10].

(2) Tuning pre-trained region embeddings to capture the tasks' focus on different features or relationships within the original urban data poses a challenge. The majority of previous urban region representation methods use simple regression models which merely projects the pre-train embeddings without capturing the specific entities and relationships relevant to individual tasks [19, 23, 24, 46, 51, 58, 59]. In contrast, prompting offers a more flexible approach by allowing models to focus on specific aspects of the data as needed [27, 41, 52], effectively highlighting small but crucial differences between urban downstream tasks. Despite this potential, existing prompting methods [48, 65] have limitations. These methods use simple prompts that do not consider detailed and heterogeneous interactions among various urban entities. Additionally, many existing prompting techniques simply concatenate prompts onto the original embeddings, lacking the flexibility to selectively filter out entities and relationships that are specifically useful for downstream tasks. This limitation makes it challenging to tailor the generalizable embedding precisely to the unique characteristics of different urban downstream tasks.

In light of the challenges discussed, we propose a novel framework named GURPP (Graph-based Urban Region Pre-training and Prompting Framework) as shown in Figure 2. Specifically:

To address the first challenge, we develop the Subgraph-centric Urban Region Pre-training (GURP) model. To capture the spatial structures and functional layouts between entities, we construct an urban region graph that integrates urban entities and their relationships. Unlike previous methods where each region is treated as a single point, our approach views each region as a subgraph.

So the GURP model then extract region subgraphs from urban region graph with graph patterns and learns region embeddings from these subgraphs through a heterogeneous graph learning model. To further enhance the learning process, we design a learning pipeline that incorporates heterogeneous graph learning model and multi-view learning. It enables the model to learn both structure information within subgraphs and the relationships between subgraphs.

To address the second challenge, we develop a knowledge-enriched prompting learning model. This model includes two approaches: a manually-designed prompt method and a task-learnable prompt learning method. The manually-designed prompt adjusts subgraph structures to highlight task-specific relationships and entities using predefined weights. The task-learnable prompt learns from task data to generate prompt graphs that capture implicit task-specific knowledge. By incorporating both predefined and learned task-specific prompts, the model tailors the general embeddings to better suit the unique characteristics and requirements of various urban computing tasks.

Contributions:

- *(Urban region graph).* We introduce urban region graph, which integrates detailed spatial and entity data for more effective urban region representation.
- *(Pre-training model).* We propose a Subgraph-centric Urban Region Pre-training (GURP) model for learning embeddings from urban region graphs, capturing generalizable patterns of interactions among entities within regions.
- *(Prompting model).* We design a novel knowledge-enriched prompting learning model with two graph-based prompting methods: a manually-defined prompt to incorporate explicit task knowledge and a task-learnable prompt to discover hidden task-relevant patterns.
- *(Extensive experiments).* We demonstrate the effectiveness of our GURPP framework through extensive experiments on three urban region prediction tasks across two cities, achieving significant performance improvements with an average increase of 17.28% on MAE and 22.26% on RMSE.

2 Preliminaries

Urban region. A city is divided into a set \mathcal{R} of non-overlapping regions based on defined criteria, such as administrative boundaries [28, 34, 46, 59] and grid partitioning [8, 21, 26, 56]. Each region $r \in \mathcal{R}$ consists of multiple spatial entities, including points of interest (POIs), roads, and junctions.

Urban region representation learning. The urban region representation learning problem involves learning a mapping function $\zeta : \mathcal{R} \rightarrow \mathbb{R}^d$, which generates a low-dimensional embedding $\vec{h} \in \mathbb{R}^d$ for each region $r \in \mathcal{R}$. This mapping considers both the spatial structures and functional layouts of the spatial entities within r , with d being the size of the embedding.

Once the mapping function $\zeta(\cdot)$ has been learned, it can be applied to various downstream prediction tasks, such as crime and check-in predictions. Let the task dataset be $\{(r_i, y_i)\}_{i=1}^{|\mathcal{R}|}$, where $y_i \in \mathbb{R}$ is a numerical indicator for region r_i . The downstream prediction tasks aim to predict y_i based on the region embedding

$\zeta(r_i)$ using a simple regression model like a Ridge Regression [15].

3 Overview

As shown in Figure 3, we propose a graph-based framework to pre-train and prompt urban region representations. Our approach begins with the creation of an urban region graph that integrates specific urban entities, providing a comprehensive structure for representing spatial and functional relationships within urban areas (discussed in Section 4.1). From this urban region graph, we extract subgraphs corresponding to each region, using graph patterns that characterize the region's structure and interactions. These subgraph representations are then refined through multi-view learning using the GURP model, enabling the capture of generalizable information that can serve as the foundation for downstream tasks (explained in Section 4.2). To tailor these representations for specific tasks, we employ two prompt-tuning methods: a manually-designed prompt method and a task-learnable prompt learning method, each designed to incorporate task-specific knowledge into the pre-trained region embeddings (elaborated in Sections 5.1 and 5.2, respectively).

4 Pre-train General Representation

In this section, we introduce the processes of constructing the urban region graph and pre-training subgraph-centric region embeddings using a multi-view learning approach.

4.1 Urban Region Graph Construction

An urban region graph is constructed to model the spatial structures and functional layouts of urban areas. The urban region graph, denoted as $G = (V, E, T_V, T_E)$, is a heterogeneous graph containing multiple types of nodes and relationships. Here, $v \in V$ and $e \in E$ represent a node and an edge, respectively, and $\phi(v) \in T_V$ ($\psi(e) \in T_E$) is a type function that assign a type to a specific node (edge).

The urban region graph follows a schema that defines the relationships among various types of nodes and edges (see Figure 4). Without loss of generality, we consider three types of spatial entities: POIs, roads, and junctions. Each spatial entity is categorized: for instance, POI categories include shops and parks, road categories encompass highways and residential streets, and junction categories cover features like roundabouts.

We construct the urban region graph from POI datasets and online maps. Since the urban region graph contains heterogeneous nodes and edges, we adopt the knowledge graph embedding technique TransR [25] to initialize the representations of all nodes and edges. This aligns the heterogeneous information into a unified vector space.

4.2 Subgraph-centric Region Embedding

We introduce a subgraph-centric region embedding model to encode the spatial structures and functional layouts of a region r .

4.2.1 Extract region-induced subgraph. The region-induced subgraph is a subgraph of G that includes the region node r and matches the graph pattern $\mathcal{P} = (P_V, P_E, \theta)$. Here, $P_V \subseteq T_V$ and $P_E \subseteq T_E$ are sets of node and edge types, respectively, which are used to filter entities and relationships specifically useful for region embeddings.

The set $\theta \subseteq T_V$ indicates the node types that serve as termination points for subgraph extraction. As a result, the schema of the region-induced subgraph is a subset of the schema of the urban region graph. During the pre-training phase, we select all node and edge types and set $P_V = T_V, P_E = T_E$, i.e., $\mathcal{P} = (T_V, T_E, \theta)$ with the aim of comprehensively characterising the rich information of a region and thereby learning general knowledge.

The region-induced subgraph $g_r = (V_r, E_r, P_V, P_E)$ includes nodes V_r and edges E_r that can be reached from r and whose types match P_V and P_E . We extract g_r recursively, starting with $V_r = \{r\}$ and $E_r = \emptyset$ and repeatedly expanding V_r and E_r until the termination points are reached. Specifically, we use a breadth-first search (BFS) starting from r to expand the subgraph. During each iteration of BFS, we explore edges $e(u, v)$ where one endpoint u is in V_r and the other endpoint v is not yet in V_r . We then check whether the type of e is in P_E and whether the type of the unseen node v is not in the termination type set θ . If e passes the checks, we add it to the set ΔE_r . Using ΔE_r , we construct the node set ΔV_r , which contains the endpoints in ΔE_r that are not already in V_r . Formally, the sets of incremental edges (i.e., ΔE_r) and nodes (i.e., ΔV_r) are as follows: $\Delta E_r = \{e(u, v) \mid u \in V_r \wedge \phi(v) \notin \theta \wedge e \in E \wedge \psi(e) \in P_E\}$ and $\Delta V_r = \{v \mid v \notin V_r \wedge \exists u \in V_r, e(u, v) \in \Delta E_r\}$. We then update the region-induced subgraph by setting $V_r = V_r \cup \Delta V_r$ and $E_r = E_r \cup \Delta E_r$. The expansion terminates if ΔE_r and ΔV_r are empty.

4.2.2 Region subgraph encoding. In Section 4.1, each node in the subgraph g_r has been assigned a global initial embedding using TransR. Here, we encode each subgraph g_r into a vector \vec{h}_r to further incorporate the local features of region r . Specifically, we use a heterogeneous graph encoder $gEnc(\cdot)$ to extract the heterogeneous and generic patterns within g_r , ultimately outputting the contextualized embedding of the subgraph.

Our encoder $gEnc(\cdot)$ chooses the Heterogeneous Graph Transformer (HGT) [17] as the subgraph node encoder due to HGT's capability of capturing node and edge-types semantics. By using HGT, $gEnc(\cdot)$ characterizes the heterogeneity of input graph by maintaining a set of node and edge-type dependent parameters, and the output embedding of each node \vec{v}^{HGT} that integrates the global initial embeddings generated by TransR, and node and edge-type semantics of the subgraph g_r . This trait aligns with our need to capture the semantic features of heterogeneous entities and relationships within each region-induced subgraph.

After obtaining the representations of each node in the subgraph, we further obtain the graph-level representation of g_r through two steps of aggregation. For each subgraph g_r , we first use $SUM(\cdot)$ function to aggregate the representations of nodes of the same type to integrate the impact of the number of entities on the representation, obtaining the node-type embedding $\vec{\tau}_i$:

$$\vec{\tau}_i = \sum_{\phi(v)=\tau_i} \vec{v}^{HGT}, \quad \tau_i \in T_V, \forall v \in V_r.$$

Then we concatenate all representations of node types, and encode them with a Linear layer to capture the interaction between various types of nodes:

$$\vec{h}_r = \text{Linear} \left(\text{CONCAT}_{|T_V|}(\vec{\tau}_i) \right).$$

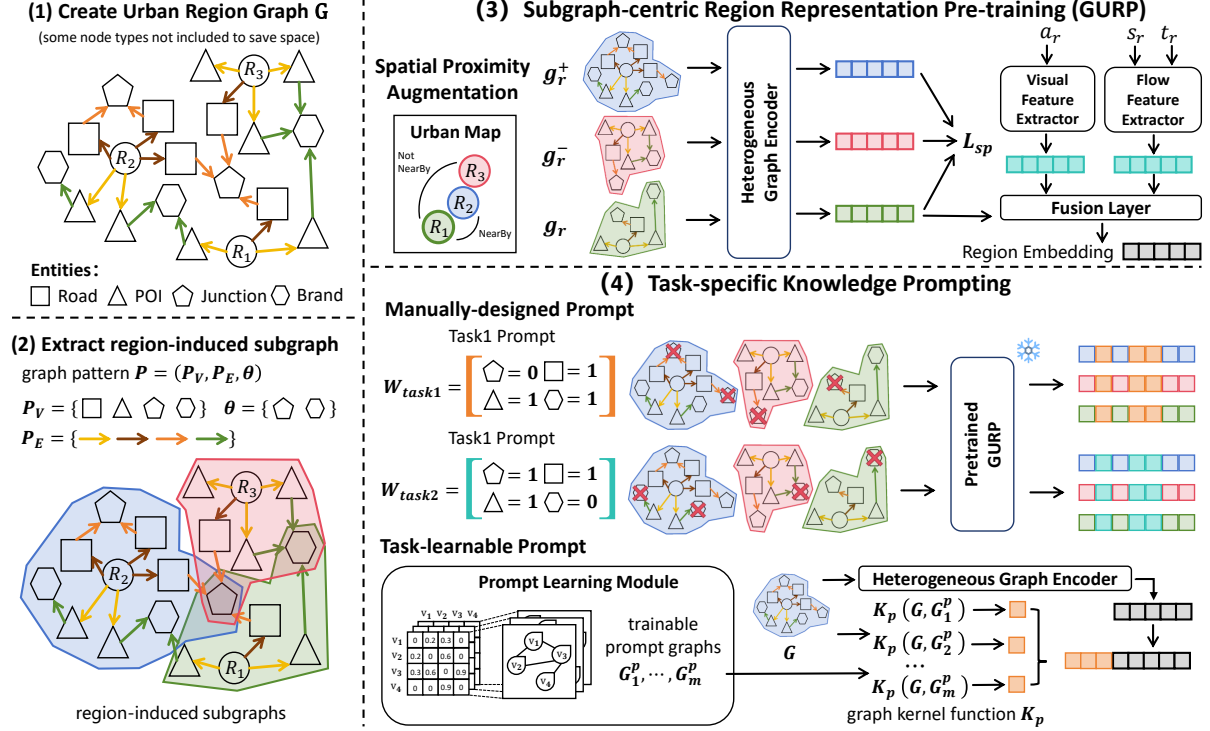


Figure 3: The Overview of our GURPP. (1) Create urban region graph that integrates specific urban entities. (2) Extract subgraph of each region according to the graph pattern. (3) Use multi-view learning to learn the subgraph representations with GURP model. (4) Adapt the region embeddings with manually-designed prompt method and task-learnable prompt learning method.

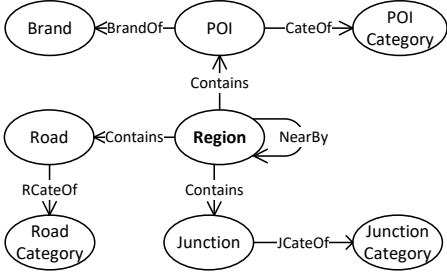


Figure 4: Schema of urban region graph.

The output \vec{h}_r of $\text{gEnc}(\cdot)$ is the final embedding of region-induced subgraph g_r . Once the graph encoder is pretrained, any graph that conforms to the pattern \mathcal{P} can be encoded by $\text{gEnc}(\cdot)$ to generate the corresponding representations, demonstrating high flexibility.

4.3 Multi-view Representation Learning

We learn the region representation with multiple views to characterize general region features by using the spatial proximity, region satellite imagery and region-wise traffic information.

4.3.1 Spatial proximity. The First Law of Geography [43] emphasizes the concept of spatial proximity, stating that “*everything is related to everything else, but near things are more related than distant things*”, which means two regions with spatial proximity should exhibit greater similarity in their representation.

We utilize a triplet network [16] to capture region similarity based on spatial proximity. For a given subgraph g_r of region r , which serves as the anchor sample, we construct its positive and negative samples based on spatial proximity. If region r' is adjacent to r (i.e., there is a “NearBy” type of edge connecting the corresponding nodes), we take the subgraph of r' as the positive sample, denoted by g_r^+ . Otherwise, we take the subgraph as the negative sample, denoted by g_r^- . We input g_r , g_r^+ , and g_r^- to the graph encoder $\text{gEnc}(\cdot)$, obtaining the vector representations \vec{h}_r , \vec{h}_r^+ , and $\vec{h}_r^- \in \mathbb{R}^d$, respectively. Then we use triplet loss to minimize the distance between adjacent regions and maximize it between distant regions, with the loss function calculated:

$$\mathcal{L}_{sp} = \sum_{r \in \mathcal{R}} \max\{||\vec{h}_r - \vec{h}_r^+||_2 - ||\vec{h}_r - \vec{h}_r^-||_2 + \delta, 0\}.$$

where δ represents the margin parameter of triplet loss.

4.3.2 Region imagery. Urban imagery encompasses various types of image information that describe the visual characteristics of a city, such as satellite images, street view images, and more. In this paper, we use satellite images as the source of urban imagery. For a given region r , its imagery can be represented as the set $\{a_1, a_2, \dots, a_m\}$. We employ a pre-trained visual model to extract visual features of the region \vec{h}_r^{img} and fuse these features with the region’s representation with the contrastive loss \mathcal{L}_{img} (see Appendix A.2 for more details).

4.3.3 Human mobility. Human mobility describes the dynamics of urban systems and is typically represented by trajectory data. For a given region r , the outflow feature \mathbf{s}_r and inflow feature \mathbf{t}_r are defined by calculating the number of outgoing and incoming trips within each time period. This results in the outflow and inflow feature sets $\{\mathbf{s}_1, \mathbf{s}_2, \dots, \mathbf{s}_N\}$ and $\{\mathbf{t}_1, \mathbf{t}_2, \dots, \mathbf{t}_N\}$, respectively, where $\mathbf{s}_i, \mathbf{t}_i \in \mathbb{R}^l$, and l is the number of intervals (e.g., 24). We then encode the inflow and outflow features using an encoder (such as a Multi-Layer Perceptron) to obtain d -dimensional embeddings:

$$\vec{h}_r^{\text{src}} = \text{Encoder}(\mathbf{s}_r), \quad \vec{h}_r^{\text{dst}} = \text{Encoder}(\mathbf{t}_r).$$

Here we adopt the reconstruction loss $\mathcal{L}_{\text{flow}}$ to optimize the two embeddings (see Appendix A.3 for more details).

4.3.4 Region representation learning. We aim to jointly learn region representations from spatial proximity, imagery, and flow views to extract general urban region knowledge and embed this into a unified representation space. To achieve this, we propose a view-fusion task that encodes the region embedding \vec{h}_r , the imagery embedding \vec{h}_r^{img} , and the flow embeddings \vec{h}_r^{src} and \vec{h}_r^{dst} into a combined vector \hat{h}_r . We then decode \hat{h}_r using separate decoders to reconstruct the original embeddings.

To implement this idea, we employ a fusion layer to integrate the embeddings: $\hat{h}_r = \text{ReLU}(\mathbf{W}[\vec{h}_r, \vec{h}_r^{\text{img}}, \vec{h}_r^{\text{src}}, \vec{h}_r^{\text{dst}}] + \mathbf{b})$, where $[\cdot]$ denotes the concatenation operation, and \mathbf{W} and \mathbf{b} are trainable weights. We design a multi-view prediction task to train the fusion layer with the loss function $\mathcal{L}_{\text{fuse}}$, defined by the ability to reconstruct the representation of each individual embedding $\vec{h}_r, \vec{h}_r^{\text{img}}, \vec{h}_r^{\text{src}}, \vec{h}_r^{\text{dst}}$ from the fused representation \hat{h}_r :

$$\mathcal{L}_{\text{fuse}} = \sum_{r \in \mathcal{R}} \sum_{k=1}^4 \|\vec{h}_r^k - \text{Decoder}^k(\hat{h}_r)\|_2^2.$$

Here, \vec{h}_r^k ($k = 1, 2, 3, 4$) represents one of the four embeddings, and Decoder^k is the corresponding decoder (such as a Multi-Layer Perceptron).

The final loss function can be formulated as follows:

$$\mathcal{L} = \mathcal{L}_{\text{sp}} + \mathcal{L}_{\text{img}} + \mathcal{L}_{\text{flow}} + \mu \mathcal{L}_{\text{fuse}}.$$

where μ is a parameter that balances the weight of the fusion loss.

5 Prompt Task-specific Knowledge

After obtaining a general region representation, a critical issue lies in how to integrate task-specific knowledge into pre-trained representations. To achieve this, we propose two graph-based prompt tuning methods: a manually-designed prompt method based on explicit domain knowledge and a task-learnable prompt learning method to extract implicit task-specific knowledge.

5.1 Manually-designed Prompt

In the manually-designed prompt, we adjust the subgraph structure, *i.e.*, defining the graph pattern $\mathcal{P}(P_V, P_E, \theta)$ in Section 4.2, to emphasize specific relationships and entities relevant to the target task, as shown in Figure 5.

We further enhance this process by manually adjusting the proportion of different types of edges and entities in the subgraph, thereby influencing the resultant embeddings. To achieve this, we

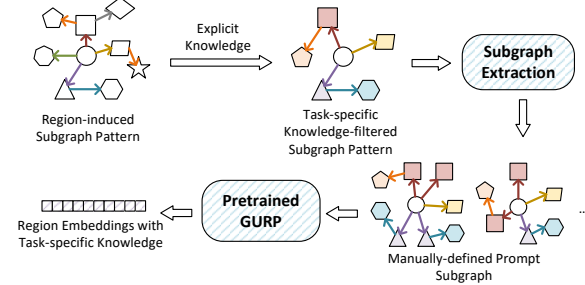


Figure 5: Manually-designed Prompt.

first define a set of task-specific entity weights \mathbf{W}_{task} that reflect the importance of various types of entities for the downstream task. These weights are designed based on domain knowledge and the specific requirements of the task. Formally, we define \mathbf{W}_{task} as:

$$\mathbf{W}_{\text{task}} = \{w_{\tau_i} \mid \tau_i \in P_V\}.$$

where P_V is the set of all possible node types in the region-induced subgraph, and $w_{\tau_i} \in [0, 1]$ represents the importance of entity type τ_i . The weights w_{τ_i} are manually defined based on domain knowledge and are used as the deletion proportion for each entity type. We define a function $\text{Adjust}(\cdot)$ to delete nodes based on \mathbf{W}_{task} : $\text{Adjust}(g_r, \mathbf{W}_{\text{task}}) \rightarrow g'_r$ where $g_r = (V_r, E_r)$ is the original subgraph. The function Adjust obtains the adjusted subgraph $g'_r = (V'_r, E'_r)$ as follows:

(1) Node Deletion: For each entity type $\tau_i \in \mathcal{E}$, delete $w_{\tau_i} \cdot |V_{\tau_i}|$ nodes of type τ_i from g_r , where $|V_{\tau_i}|$ is the number of nodes of type τ_i in g_r , such that $V'_r = V_r \setminus \{v \mid \phi(v) = \tau_i\}$ with probability $1 - w_{\tau_i}$.

(2) Edge Deletion: After node deletion, delete edges connected to the removed nodes, such that $E'_r = \{e \mid e = (u, v) \in E; u, v \in V'_r\}$.

The adjusted subgraph $g'_r = (V'_r, E'_r)$ is then input to the pre-trained GURP to generate the task-specific embeddings.

In summary, the manually-designed prompt is the graph pattern \mathcal{P} with the set of task-specific entity weights \mathbf{W}_{task} , which guide the $\text{Adjust}(\cdot)$ function in modifying the subgraph g_r to g'_r . By incorporating these manually-designed prompts, we can tailor the urban region representations to better capture task-relevant entities and relationships. This approach also offers the advantage of adapting to downstream tasks without the need for additional training. It simply requires adjusting the input subgraph based on the manually-defined prompts.

5.2 Task-learnable Prompt

Apart from leveraging explicitly designed task-specific knowledge prompts to enrich region representations, in the presence of sufficient task data, we can also learn prompts based on the task data and pre-trained representations to induce implicit knowledge within the task data, thereby enhancing region representations.

Considering that we describe the attributes of an urban region through subgraph induced with region nodes from G , it is intuitive to similarly describe the task adaptation to different region attributes with graphs as well. Therefore, we propose a prompt learning module to use prompt graphs to portray the adaptation

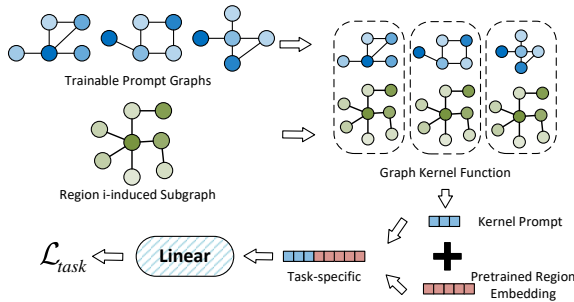


Figure 6: Task-learnable Prompt.

of downstream task relative to the original region embedding, as shown in Figure 6.

We introduce the graph kernel method [7, 33, 44] to assess the similarity of between the prompt graphs and the region subgraphs due to its excellent performance and computational efficiency, then enhancing the pre-trained region embedding. Let \mathcal{G} denote the prompt graph set consisting of m trainable (hidden) prompt graphs, where each prompt graph $G^p \in \mathcal{G}$ is defined as $G^p = (V^p, E^p, X^p)$. Here, $X^p \in \mathbb{R}^{|V^p| \times d}$ represents the node attributes, with d being the dimension of these attributes. For each region subgraph g_r , we utilize an attribute graph kernel function $K_p(\cdot, \cdot)$ to measure the similarity between g_r and each prompt graph $G_1^p, G_2^p, \dots, G_m^p$. Specifically, we employ the P -step random walk kernel (more details in Appendix A.4) to compute the kernel value between the region subgraph g_r and each prompt graph G_i^p . These values are concatenated to form an m -dimensional prompt vector $\vec{h}_p \in \mathbb{R}^m$ for each region. We concatenate the prompt vector $\vec{h}_p \in \mathbb{R}^m$ before the pre-trained region representation \vec{h}_r to derive region embedding $\vec{h}'_r = \vec{h}_p || \vec{h}_r$. The new embeddings are then fed into a linear layer $\text{Linear}(\cdot)$. We update the prompt graphs and linear layer parameters, by optimizing on the downstream labeled task, to obtain the final prompt representation with the simple MSE loss function:

$$\mathcal{L}_{\text{task}} = \frac{1}{N} \sum_{i=1}^N (y_i^{\text{pred}} - y_i^{\text{label}})^2.$$

6 Experiments

We conduct extensive experiments to investigate the following research questions (RQs):

- **RQ1:** Can our proposed pre-train and prompt framework (GURPP) outperform previous approaches?
- **RQ2:** Does GURP have the ability to capture and apply heterogeneous and generic patterns?
- **RQ3:** How does the manually-designed prompt work?
- **RQ4:** How does the task-learnable prompt perform and how does it look like?
- **RQ5:** How does each component contribute to GURPP?

6.1 Experimental Setup

6.1.1 Datasets. We collect the datasets of region division, POI, urban imagery, taxi trips, road network, check-in, crime and crash for two representative cities in the United States: New York City (NYC) and Chicago (CHI). The detailed statistics and sources of the dataset is available in Appendix A.5.

6.1.2 Baselines. We compare our model with the following representative baseline models: knowledge graph embedding methods and its variants (**TransR** [25], **TransR-N**, **TransR-G**), graph embedding methods (**node2vec** [12], **GAE** [22]), and urban region embedding methods (**MVURE** [59], **MGFN** [46], **HREP** [65], **HRE**, **ReCP** [24]). These baselines cover the range from traditional graph embedding to complex models that take into account urban-specific attributes, providing us with a comprehensive performance comparison benchmark. Specific details and descriptions can be found in the Appendix A.6.

6.1.3 Metrics and Implementation. To evaluate the prediction performance, we use three widely recognized evaluation metrics: the coefficient of determination (R^2), root mean squared error (RMSE), and mean absolute error (MAE). Better performance is indicated by a higher R^2 and lower RMSE and MAE values. Our model includes three version: 1) GURP represents the pre-train module, 2) GURPP_M is GURP with manually-designed prompt, and 3) GURPP_T is GURP with task-learnable prompt. For detailed implementation, please refer to Appendix A.7 and our provided code repository.

6.2 RQ1 & RQ2: Overall Performance

We evaluate the overall performance of baselines and our model on three downstream tasks. The results of the experiments are shown in Table 1, where the GURPP is all implemented by GURPP_T. From the results, we find the following:

(1) GURPP demonstrates superior performance to baselines in both pre-training and prompting phases. In the pre-training phase, the performance of GURP improves by 6.54%, 8.28%, 462.03%, and 113.01% over the best baseline of R^2 on two urban datasets. Meanwhile, on all downstream tasks, the average performance on MAE and RMSE metrics improves by 17.28% and 22.26%, respectively. Subsequently, the performance of GURPP is further improved by an average of 9.50%, 9.28%, and 11.703% of MAE, RMSE and R^2 , respectively, when we introduce the task-learnable prompt. The results validate the significant advantages of our proposed pre-train and prompt framework.

(2) To validate the ability of our pre-training method to capture generic urban knowledge, we compare the performance of state-of-the-art urban region embedding methods on datasets from two distinct cities, NYC and CHI. The results show that while these baselines perform well on the NYC dataset, their performance drops significantly on the CHI dataset. For instance, the performance on CHI decreases by an average of 71.8% in R^2 compared to NYC. In contrast, our GURPP model demonstrates remarkable consistency, with only an 8.49% decrease in R^2 . This may be due to the fact that the baselines tend to be effective only at extracting information specific to certain data types, but they do not consider spatial structure and functional layouts among urban entities. For example, existing baselines rely on the flow view to extract information. However, the content of flow view in the CHI dataset is sparse, leading to a significant degradation in the performance of downstream task.

Table 1: Main performance comparison of different models on downstream tasks across NYC and CHI datasets. The best results for each metric are highlighted in bold, the second-best are underlined, and the third-best are marked with an asterisk. The last and the third-to-last rows show the percentage improvement of the GURPP and GURP models over the third-best model.

Model	New York City (NYC)						Chicago (CHI)					
	Crime Prediction			Check-in Prediction			Crime Prediction			Crash Prediction		
	MAE	RSME	R^2	MAE	RSME	R^2	MAE	RSME	R^2	MAE	RSME	R^2
TransR-N	111.319	148.863	-0.014	534.699	805.282	0.031	209.072	307.454	-0.037	106.914	176.860	0.001
TransR-G	109.221	146.905	0.013	530.427	802.426	0.038	208.404	306.155	-0.028	104.680	174.419	0.028
node2vec	138.458	175.797	-0.414	573.118	837.441	-0.048	246.066	349.965	-0.343	121.900	174.907	0.023
GAE	96.846	126.364	0.270	349.942	542.920	0.560	200.606*	300.237	0.011	100.536	173.323	0.040
MVURE	72.471*	99.844	0.544	310.973	498.076	0.629	206.080	289.859*	0.079*	96.953	148.865*	0.292*
MGFN	73.502	97.440*	0.566*	300.150	456.626*	0.688*	214.021	310.832	-0.059	108.3740	179.854	-0.033
HRE	76.926	102.07	0.523	329.547	513.801	0.606	206.612	298.389	0.024	99.952	158.625	0.196
HREP	74.854	100.035	0.542	320.335	505.516	0.618	206.591	298.238	0.025	99.766	158.658	0.196
ReCP	73.853	100.558	0.537	292.871*	524.890	0.588	207.485	298.965	0.020	93.298*	157.515	0.207
GURP	72.094	<u>93.216</u>	<u>0.603</u>	<u>271.689</u>	<u>412.918</u>	<u>0.745</u>	<u>161.266</u>	<u>225.244</u>	<u>0.444</u>	<u>80.362</u>	<u>108.781</u>	<u>0.622</u>
Enhance	0.52%	4.33%	6.54%	7.23%	9.57%	8.28%	19.61%	22.29%	462.03%	13.87%	26.93%	113.01%
GURPP	71.481	91.612	0.616	261.450	388.225	0.775	146.385	203.050	0.548	65.297	92.114	0.729
Enhance	1.36%	5.98%	8.83%	10.73%	14.98%	12.65%	27.03%	29.95%	593.67%	30.01%	38.12%	149.66%

While GURPP shows excellent performance on both urban datasets, which demonstrates the robustness and universality of GURPP across diverse urban environments.

(3) To further validate the effectiveness of our subgraph-centric and multi-view fusion module, we conduct experiments comparing the performance of models with and without subgraphs and multi-view fusion. Specifically, we compare the TransR-G model (adopts region-induced subgraph and regards graph-level embedding as the region embedding) with the TransR-N model (directly uses region nodes embedding as region embedding). The results indicate that TransR-G outperforms TransR-N by an average of 1.27% in MAE, underscoring the effectiveness of the subgraph-centered approach. This improvement is attributed to the subgraph-centric method's ability to better preserve the structural and contextual information of regions, providing more accurate and meaningful urban region embeddings. The average 32.55% improvement in MAE for GURP over TransR-G is mainly due to the multi-view fusion strategy, which improves the model's comprehensive understanding of urban features.

6.3 RQ3: Manually-designed Prompt Study

In the real world, the incidence of crime is often closely linked to specific POI categories, roads and junctions, for example, ATMs, bars, parks, etc. are more likely to be the location of a crime. The density of roads and the complexity of junctions are also important factors affecting crime rates. As for the check-in behavior, the brand of the POI is given more attention, and certain users may be more inclined to check in at locations of well-known brands such as Starbucks, McDonald's, or other specific brands. Therefore, we designed two patterns as shown in Figure 7 to validate the performance of manually-designed prompt.

The results are shown in Table 2, from which it can be found that crime prediction does pay more attention to factors such as POI

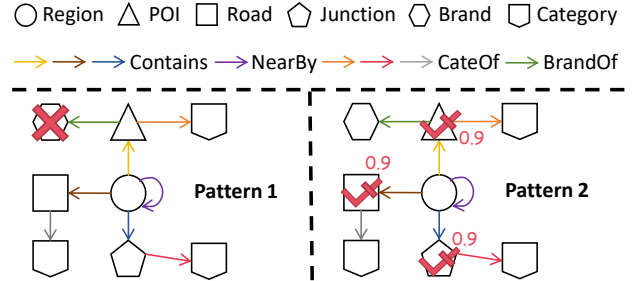


Figure 7: The structure of the manually-designed prompt based on Pattern 1 (P1) and Pattern 2 (P2). P1 ignores POI brand information. P2 randomly samples POI, road, and junction nodes around the region with a weight of 0.9.

categories, roads and junctions, which are closely related to criminal behavior. Meanwhile, removing POI brand information shows a significant decrease in the performance of check-in prediction. These results also demonstrate that the prediction performance of the model can be improved by manually-designed prompt.

Table 2: Performance of GURPP_M.

Model	Crime Prediction (NYC)			Check-in Prediction (NYC)		
	MAE	RSME	R^2	MAE	RSME	R^2
GURP	72.094	93.216	0.603	271.689	412.918	0.745
GURPP _M -P1	68.538	88.698	0.640	273.201	429.564	0.724
GURPP _M -P2	69.421	91.834	0.614	262.437	397.466	0.764

6.4 RQ4: Task-learnable Prompt Study

6.4.1 Effectiveness of Task-learnable Prompt. We utilize GURP pre-trained embedding with the simple prefix prompt (proposed by HREP[65]) and task-learnable prompt respectively for comparative

Table 3: Effectiveness of Task-learnable Prompt.

Framework	Crime Prediction (NYC)			Crash Prediction (CHI)		
	MAE	RSME	R^2	MAE	RSME	R^2
GURP	72.094	93.216	0.603	80.362	108.781	0.622
GURP+Pre	73.758	93.971	0.596	66.330	93.772	0.719
GURPP _T	71.481	91.612	0.616	65.297	92.114	0.729

**Figure 8: Visualization of learned prompt graphs.**

analysis. Both of these prompt methods are data-driven and seek to improve the region representation by learning data for specific downstream tasks. We conduct experiments on crime prediction task in NYC and crash prediction task in CHI, respectively, and the results are shown in Table 3.

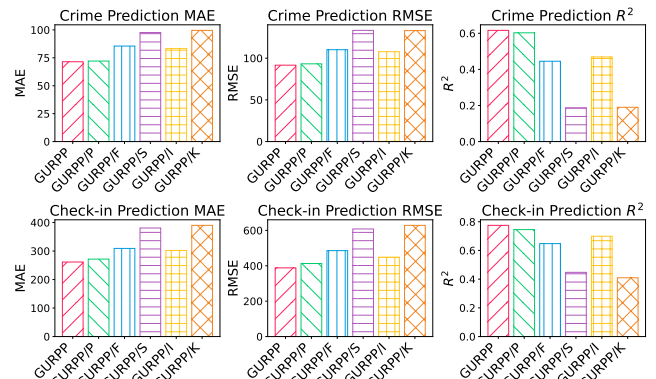
Our task-learnable prompt outperforms pre-trained embeddings across both tasks, with improvements of 8.83% of R^2 in crime prediction and 149.66% of R^2 in crash prediction, indicating that the prompt is highly effective in providing tailored guidelines for different downstream tasks. However, in crime prediction task, the prefix prompt have an negative effect, resulting in a performance decrease of 1.16% of R^2 . This demonstrates that our task-learnable prompt is more stable and effective compared to prefix prompt.

6.4.2 Visualization of Learned Prompt Graph. Compared to prefix prompt, our task-learnable prompt is able to generate a series of prompt graphs during training, which enhances the clarity of our prompt method. We visualize prompt graphs that reveal key structural features in the urban region graph of interest in the task. In Figure 8, we show some prompt graphs for crime prediction tasks in CHI. (Additional prompt graphs can be found in Appendix A.8.) These results show that the prompt graphs generally exhibits circular structural features, implying that the model have identified and emphasized interactions between urban entities.

6.5 RQ5: Ablation Studies

Finally, we conduct the ablation studies in NYC dataset to investigate the effectiveness of the individual components of GURPP. Variants of GURPP are designed as follows: **GURPP/P**. We use only the pre-training process to learn urban region general representation. **GURPP/F**, **GURPP/S**, **GURPP/I**. We remove the flow view, spatial proximity view, and imagery view from GURPP, respectively. **GURPP/K**. We replace the knowledge graph embedding initialization with random initialization.

Figure 9 presents the ablation results of our model and its variants. Spatial proximity view and knowledge graph embedding method significantly enhance the model's performance, lifting it by 151.64% and 156.67% of R^2 , respectively. These components effectively capture the heterogeneous and generic patterns of interactions among entities by elucidating the spatial relationships and structured knowledge of the urban region. The flow view and

**Figure 9: Results of ablation studies.**

the imagery view can also greatly enhance the performance of the model, increasing it by 29.04% and 21.11%, respectively. This is because they capture dynamic flow information and visual features of urban regions, respectively, providing the model with a multi-dimensional context that enhances its ability to fully understand and predict urban dynamics. Prompt learning, with an improvement of 3.12%, effectively elevates model performance by introducing guiding prompts that allow the model to delve deeper into understanding and utilizing task-relevant knowledge.

7 Related Work

Extensive studies have been conducted to learn urban region representation from different perspectives. We combine the existing work categories in Table 4.

Table 4: Cats.of Related Works on Urban Region Embedding

Methods	Task-specific learning or fine-tuning	Prompting
Non-graph	[19, 23, 24, 50, 51, 58, 66]	[48, 56, 65]
Graph	[2, 13, 28, 34, 46, 47, 59, 60]	GURPP(Ours)

Task-specific learning or fine-tuning. Urban region representation learning aims to extract complex patterns and relationships within urban regions and embed them into a representation space. Existing research can be broadly classified into two categories: task-specific supervised region representation learning [2, 13, 50, 66] and general unsupervised region representation learning [19, 23, 24, 46, 51, 58, 59]. These works utilize feature aggregation models to generate representation from predefined region statistics with limitations in capturing detailed spatial layout and semantics. Moreover, using predefined statistical features makes it challenging to further adapt the representation to the specificities of various downstream tasks. We address the limitations by leveraging a urban region graph and subgraph-centric region embeddings, which learn the generic knowledge of urban spatial layout and generate flexible region representation tailored to different tasks.

Pre-training and Prompting. Recent years have witnessed the significant success of pre-training and prompting paradigm in fields of NLP [4, 11, 27, 39], CV [38, 52, 63, 64] and graph learning [31, 41, 53, 54]. Many works in urban computing have also made attempts in this regard [3, 47, 48, 56, 60]. For instance, Yuan *et al.* [56] design an urban spatio-temporal prediction pre-train

and prompt model. Yan *et al.* [48] introduce large language models (LLMs) to describe urban imagery features and unify different prediction tasks through textual prompts. However, the urban tasks explored in these work differ from ours, with a distinct focus. Our work can also benefit from the integration of LLMs to enhance fine-grained characterization capabilities. As a similar work, HREP [65] introduces prefix prompt to region embedding, but the pre-trained model fails to adequately capture the fine-grained features of regions. We propose both manually-designed and task-learnable prompts built on graph-based pre-train model to address this issue.

8 Conclusion and Future Works

In this paper, we introduce the urban region graph and propose a graph-based pre-training and prompting framework for urban region representation learning, balancing urban generality and task specificity. We develop a subgraph-centric pre-training model to capture general urban knowledge and two prompt methods to incorporate task-specific insights. Extensive experiments demonstrate the effectiveness of our approach. Future work may explore: 1) Integrating textual data and LLMs to uncover more universal urban knowledge; 2) Developing arbitrary region representations for flexible urban modeling; 3) Assessing the transferability of urban representations across cities to enhance general applicability.

References

- [1] Arcgis 2024. *ArcGIS Online*. Retrieved July 28, 2024 from <https://www.arcgis.com/index.html>
- [2] Lei Bai, Lina Yao, Salil S Kanhere, Xianzhi Wang, Wei Liu, and Zheng Yang. 2019. Spatio-temporal graph convolutional and recurrent networks for citywide passenger demand prediction. In *Proceedings of the 28th ACM international conference on information and knowledge management (CIKM)*. 2293–2296.
- [3] Pasquale Balsebre, Weiming Huang, Gao Cong, and Yi Li. 2023. City Foundation Models for Learning General Purpose Representations from OpenStreetMap. *arXiv preprint arXiv:2310.00583* (2023).
- [4] Tom Brown, Benjamin Mann, Nick Ryder, Melanie Subbiah, Jared D Kaplan, Prafulla Dhariwal, Arvind Neelakantan, Pranav Shyam, Girish Sastry, Amanda Askell, et al. 2020. Language models are few-shot learners. In *Advances in neural information processing systems (NeurIPS)*, Vol. 33. 1877–1901.
- [5] Census Bureau 2024. *Measuring America's People, Places, and Economy*. Retrieved July 28, 2024 from <https://www.census.gov/>
- [6] Chicago Data Portal 2024. *Chicago Data Portal*. Retrieved July 28, 2024 from <https://data.cityofchicago.org/>
- [7] Aosong Feng, Chenyu You, Shiqiang Wang, and Leandros Tassiulas. 2022. Kergnns: Interpretable graph neural networks with graph kernels. In *Proceedings of the AAAI conference on artificial intelligence (AAAI)*, Vol. 36. 6614–6622.
- [8] Kaiyu Feng, Gao Cong, Christian S Jensen, and Tao Guo. 2019. Finding attribute-aware similar region for data analysis. *Proceedings of the VLDB Endowment* 12, 11 (2019), 1414–1426.
- [9] Foursquare 2024. *What can Foursquare do for you?* Retrieved July 28, 2024 from <https://data.cityofchicago.org/>
- [10] Yanjie Fu, Pengyang Wang, Jiadi Du, Le Wu, and Xiaolin Li. 2019. Efficient region embedding with multi-view spatial networks: A perspective of locality-constrained spatial autocorrelations. In *Proceedings of the AAAI Conference on Artificial Intelligence (AAAI)*, Vol. 33. 906–913.
- [11] Tianyu Gao, Adam Fisch, and Danqi Chen. 2021. Making Pre-trained Language Models Better Few-shot Learners. In *Proceedings of the 59th Annual Meeting of the Association for Computational Linguistics and the 11th International Joint Conference on Natural Language Processing (ACL/IJCNLP)*. 3816–3830.
- [12] Aditya Grover and Jure Leskovec. 2016. node2vec: Scalable feature learning for networks. In *Proceedings of the 22nd ACM SIGKDD international conference on Knowledge discovery and data mining (KDD)*. 855–864.
- [13] Haoyu Han, Mengdi Zhang, Min Hou, Fuzheng Zhang, Zhongyuan Wang, Enhong Chen, Hongwei Wang, Jianhui Ma, and Qi Liu. 2020. STGCN: a spatial-temporal aware graph learning method for POI recommendation. In *2020 IEEE International Conference on Data Mining (ICDM)*. 1052–1057.
- [14] Kaiming He, Xiangyu Zhang, Shaoqing Ren, and Jian Sun. 2016. Deep residual learning for image recognition. In *Proceedings of the IEEE conference on computer vision and pattern recognition (CVPR)*. 770–778.
- [15] Arthur E Hoerl and Robert W Kennard. 1970. Ridge regression: Biased estimation for nonorthogonal problems. *Technometrics* 12, 1 (1970), 55–67.
- [16] Elad Hoffer and Nir Ailon. 2015. Deep metric learning using triplet network. In *Similarity-based pattern recognition: third international workshop (SIMBAD)*. Springer, 84–92.
- [17] Ziniu Hu, Yuxiao Dong, Kuansan Wang, and Yizhou Sun. 2020. Heterogeneous graph transformer. In *Proceedings of the web conference 2020 (WWW)*. 2704–2710.
- [18] Bo Hui, Da Yan, Wei-Shinn Ku, and Wenlu Wang. 2020. Predicting economic growth by region embedding: A multigraph convolutional network approach. In *Proceedings of the 29th ACM International Conference on Information & Knowledge Management*. 555–564.
- [19] Porter Jenkins, Ahmad Farag, Suhang Wang, and Zhenhui Li. 2019. Unsupervised representation learning of spatial data via multimodal embedding. In *Proceedings of the 28th ACM international conference on information and knowledge management (CIKM)*. 1993–2002.
- [20] Xunqiang Jiang, Tianrui Jia, Yuan Fang, Chuan Shi, Zhe Lin, and Hui Wang. 2021. Pre-training on large-scale heterogeneous graph. In *Proceedings of the 27th ACM SIGKDD conference on knowledge discovery & data mining*. 756–766.
- [21] Jiahui Jin, Yifan Song, Dong Kan, Binjie Zhang, Yan Lyu, Jinghui Zhang, and Hongru Lu. 2024. Learning context-aware region similarity with effective spatial normalization over Point-of-Interest data. *Information Processing & Management* 61, 3 (2024), 103673.
- [22] Thomas N Kipf and Max Welling. 2016. Variational graph auto-encoders. *arXiv preprint arXiv:1611.07308* (2016).
- [23] Yi Li, Weiming Huang, Gao Cong, Hao Wang, and Zheng Wang. 2023. Urban region representation learning with OpenStreetMap building footprints. In *Proceedings of the 29th ACM SIGKDD Conference on Knowledge Discovery and Data Mining (KDD)*. 1363–1373.
- [24] Zechen Li, Weiming Huang, Kai Zhao, Min Yang, Yongshun Gong, and Meng Chen. 2024. Urban Region Embedding via Multi-View Contrastive Prediction. In *Proceedings of the AAAI Conference on Artificial Intelligence (AAAI)*, Vol. 38. 8724–8732.
- [25] Yankai Lin, Zhiyuan Liu, Maosong Sun, Yang Liu, and Xuan Zhu. 2015. Learning entity and relation embeddings for knowledge graph completion. In *Proceedings of the AAAI conference on artificial intelligence (AAAI)*, Vol. 29. 2181–2187.
- [26] Lingbo Liu, Zhihui Qiu, Guanbin Li, Qing Wang, Wanli Ouyang, and Liang Lin. 2019. Contextualized spatial-temporal network for taxi origin-destination demand prediction. *IEEE Transactions on Intelligent Transportation Systems* 20, 10 (2019), 3875–3887.
- [27] Pengfei Liu, Weizhe Yuan, Jinlan Fu, Zhengbao Jiang, Hiroaki Hayashi, and Graham Neubig. 2023. Pre-train, prompt, and predict: A systematic survey of prompting methods in natural language processing. *Comput. Surveys* 55, 9 (2023), 1–35.
- [28] Yu Liu, Jingtao Ding, Yanjie Fu, and Yong Li. 2023. Urbang: An urban knowledge graph system. *ACM Transactions on Intelligent Systems and Technology* 14, 4 (2023), 1–25.
- [29] Yu Liu, Xin Zhang, Jingtao Ding, Yanxin Xi, and Yong Li. 2023. Knowledge-infused contrastive learning for urban imagery-based socioeconomic prediction. In *Proceedings of the ACM Web Conference 2023 (WWW)*. 4150–4160.
- [30] Yan Luo, Fu-lai Chung, and Kai Chen. 2022. Urban region profiling via multi-graph representation learning. In *Proceedings of the 31st ACM International Conference on Information & Knowledge Management*. 4294–4298.
- [31] Yihong Ma, Ning Yan, Jiayu Li, Masood Mortazavi, and Nitesh V Chawla. 2024. Hetgpt: Harnessing the power of prompt tuning in pre-trained heterogeneous graph neural networks. In *Proceedings of the ACM on Web Conference 2024 (WWW)*. 1015–1023.
- [32] Nikhil Naik, Jade Philipoom, Ramesh Raskar, and César Hidalgo. 2014. Streetscore: predicting the perceived safety of one million streetscapes. In *Proceedings of the IEEE conference on computer vision and pattern recognition workshops*. 779–785.
- [33] Giannis Nikolenzios and Michalis Vazirgiannis. 2020. Random walk graph neural networks. In *Advances in Neural Information Processing Systems (NeurIPS)*, Vol. 33. 16211–16222.
- [34] Yansong Ning, Hao Liu, Hao Wang, Zhenyu Zeng, and Hui Xiong. 2024. UUKG: unified urban knowledge graph dataset for urban spatiotemporal prediction. In *Advances in Neural Information Processing Systems (NeurIPS)*, Vol. 36. 62442–62456.
- [35] NYC OpenData 2024. *Open Data for All New Yorkers*. Retrieved July 28, 2024 from <https://opendata.cityofnewyork.us/>
- [36] OpenStreetMap 2024. *OpenStreetMap*. Retrieved July 28, 2024 from <https://www.openstreetmap.org/>
- [37] Sungwon Park, Sungwon Han, Donghyun Ahn, Jaeyeon Kim, Jeasurk Yang, Su-sang Lee, Seunghoon Hong, Jihee Kim, Sangyoon Park, Hyunjoo Yang, et al. 2022. Learning economic indicators by aggregating multi-level geospatial information. In *Proceedings of the AAAI Conference on Artificial Intelligence*, Vol. 36. 12053–12061.

[38] Alec Radford, Jong Wook Kim, Chris Hallacy, Aditya Ramesh, Gabriel Goh, Sandhini Agarwal, Girish Sastry, Amanda Askell, Pamela Mishkin, Jack Clark, et al. 2021. Learning transferable visual models from natural language supervision. In *International conference on machine learning (ICML)*. 8748–8763.

[39] Adam Roberts, Colin Raffel, and Noam Shazeer. 2020. How Much Knowledge Can You Pack Into the Parameters of a Language Model?. In *Proceedings of the 2020 Conference on Empirical Methods in Natural Language Processing (EMNLP)*. 5418–5426.

[40] Safegraph 2024. *Your Partner in Places Data*. Retrieved July 28, 2024 from <https://www.safegraph.com/>

[41] Xiangguo Sun, Hong Cheng, Jia Li, Bo Liu, and Jihong Guan. 2023. All in one: Multi-task prompting for graph neural networks. In *Proceedings of the 29th ACM SIGKDD Conference on Knowledge Discovery and Data Mining (KDD)*. 2120–2131.

[42] Jian Tang, Meng Qu, Mingzhe Wang, Ming Zhang, Jun Yan, and Qiaozhu Mei. 2015. Line: Large-scale information network embedding. In *Proceedings of the 24th international conference on world wide web*. 1067–1077.

[43] Waldo R Tobler. 1970. A computer movie simulating urban growth in the Detroit region. *Economic geography* 46, sup1 (1970), 234–240.

[44] S Vichy N Vishwanathan, Nicol N Schraudolph, Risi Kondor, and Karsten M Borgwardt. 2010. Graph kernels. *The Journal of Machine Learning Research* 11 (2010), 1201–1242.

[45] Hongjian Wang and Zhenhui Li. 2017. Region representation learning via mobility flow. In *Proceedings of the 2017 ACM on Conference on Information and Knowledge Management (CIKM)*. 237–246.

[46] Shangbin Wu, Xu Yan, Xiaoliang Fan, Shirui Pan, Shichao Zhu, Chuanpan Zheng, Ming Cheng, and Cheng Wang. 2022. Multi-graph fusion networks for urban region embedding. In *Proceedings of the Thirty-First International Joint Conference on Artificial Intelligence (IJCAI)*. 2312–2318.

[47] Fengli Xu, Jun Zhang, Chen Gao, Jie Feng, and Yong Li. 2023. Urban generative intelligence (ugi): A foundational platform for agents in embodied city environment. *arXiv preprint arXiv:2312.11813* (2023).

[48] Yibo Yan, Haomin Wen, Siru Zhong, Wei Chen, Haodong Chen, Qingsong Wen, Roger Zimmermann, and Yuxuan Liang. 2024. Urbanelip: Learning text-enhanced urban region profiling with contrastive language-image pretraining from the web. In *Proceedings of the ACM on Web Conference 2024 (WWW)*. 4006–4017.

[49] Dingqi Yang, Daqing Zhang, Vincent W Zheng, and Zhiyong Yu. 2014. Modeling user activity preference by leveraging user spatial temporal characteristics in LBSNs. *IEEE Transactions on Systems, Man, and Cybernetics: Systems* 45, 1 (2014), 129–142.

[50] Min Yang, Bo Kong, Ruirong Dang, and Xiongfeng Yan. 2022. Classifying urban functional regions by integrating buildings and points-of-interest using a stacking ensemble method. *International Journal of Applied Earth Observation and Geoinformation* 108 (2022), 102753.

[51] Zijun Yao, Yanjie Fu, Bin Liu, Wangsu Hu, and Hui Xiong. 2018. Representing urban functions through zone embedding with human mobility patterns. In *Proceedings of the Twenty-Seventh International Joint Conference on Artificial Intelligence (IJCAI)*. 3919–3925.

[52] Seungryong Yoo, Eunji Kim, Dahuin Jung, Jungbeom Lee, and Sungroh Yoon. 2023. Improving visual prompt tuning for self-supervised vision transformers. In *International Conference on Machine Learning (ICML)*. 40075–40092.

[53] Xingtong Yu, Yuan Fang, Zemin Liu, and Xinming Zhang. 2024. Hgprompt: Bridging homogeneous and heterogeneous graphs for few-shot prompt learning. In *Proceedings of the AAAI Conference on Artificial Intelligence (AAAI)*, Vol. 38. 16578–16586.

[54] Xingtong Yu, Chang Zhou, Yuan Fang, and Xinming Zhang. 2024. MultiGPrompt for multi-task pre-training and prompting on graphs. In *Proceedings of the ACM on Web Conference 2024 (WWW)*. 515–526.

[55] Jing Yuan, Yu Zheng, and Xing Xie. 2012. Discovering regions of different functions in a city using human mobility and POIs. In *Proceedings of the 18th ACM SIGKDD international conference on Knowledge discovery and data mining*. 186–194.

[56] Yuan Yuan, Jingtao Ding, Jie Feng, Depeng Jin, and Yong Li. 2024. UniST: A Prompt-Empowered Universal Model for Urban Spatio-Temporal Prediction. *arXiv preprint arXiv:2402.11838* (2024).

[57] Wei Zhai, Xueyin Bai, Yu Shi, Yu Han, Zhong-Ren Peng, and Chaolin Gu. 2019. Beyond Word2vec: An approach for urban functional region extraction and identification by combining Place2vec and POIs. *Computers, environment and urban systems* 74 (2019), 1–12.

[58] Liang Zhang, Cheng Long, and Gao Cong. 2023. Region embedding with intra and inter-view contrastive learning. *IEEE Transactions on Knowledge and Data Engineering* 35, 9 (2023), 9031–9036.

[59] Mingyang Zhang, Tong Li, Yong Li, and Pan Hui. 2021. Multi-view joint graph representation learning for urban region embedding. In *Proceedings of the Twenty-Ninth International Conference on International Joint Conferences on Artificial Intelligence (IJCAI)*. 4431–4437.

[60] Weijia Zhang, Jindong Han, Zhao Xu, Hang Ni, Hao Liu, and Hui Xiong. 2024. Towards Urban General Intelligence: A Review and Outlook of Urban Foundation Models. *arXiv preprint arXiv:2402.01749* (2024).

[61] Yunchao Zhang, Yanjie Fu, Pengyang Wang, Xiaolin Li, and Yu Zheng. 2019. Unifying inter-region autocorrelation and intra-region structures for spatial embedding via collective adversarial learning. In *Proceedings of the 25th ACM SIGKDD International Conference on Knowledge Discovery & Data Mining*. 1700–1708.

[62] Yunxiang Zhao, Jianzhong Qi, Bayu D Trisedy, Yixin Su, Rui Zhang, and Hongguang Ren. 2023. Learning region similarities via graph-based deep metric learning. *IEEE Transactions on Knowledge and Data Engineering* 35, 10 (2023), 10237–10250.

[63] Kaiyang Zhou, Jingkang Yang, Chen Change Loy, and Ziwei Liu. 2022. Conditional prompt learning for vision-language models. In *Proceedings of the IEEE/CVF conference on computer vision and pattern recognition (CVPR)*. 16816–16825.

[64] Kaiyang Zhou, Jingkang Yang, Chen Change Loy, and Ziwei Liu. 2022. Learning to prompt for vision-language models. *International Journal of Computer Vision* 130, 9 (2022), 2337–2348.

[65] Silin Zhou, Dan He, Lisi Chen, Shuo Shang, and Peng Han. 2023. Heterogeneous region embedding with prompt learning. In *Proceedings of the AAAI Conference on Artificial Intelligence (AAAI)*, Vol. 37. 4981–4989.

[66] Zhengyang Zhou, Kuo Yang, Yuxuan Liang, Binwu Wang, Hongyang Chen, and Yang Wang. 2023. Predicting collective human mobility via counteracting spatiotemporal heterogeneity. *IEEE Transactions on Mobile Computing* 23, 5 (2023), 4723–4738.

A Appendix

A.1 Appendix of urban region graph construction

Here we provide more details for the urban region graph construction. Specifically, we incorporate brand information for POI entities, such as Starbucks, to enhance the representation of POI functionalities. Altogether, we define eight node types shared across regions and cities: *region*, *POI*, *POI category*, *brand*, *road*, *road category*, *junction*, and *junction category*, comprising the node type set T_V . We also define six edge types, forming the edge type set T_E . These include the *NearBy* relationship, which connects region entities based on their geographical adjacency; the *Contains* relationship, which is based on spatial containment; the *BrandOf* relationship, which links brands to POI entities; and the *CateOf*, *JCateOf*, and *RCateOf* relationships, which are based on the category information of the entities.

A.2 Appendix of region imagery encoding

We supplement more details for the urban imagery encoding. Specifically, we employ ResNet [14] to extract visual features for each region image, such that $\vec{a}_k = \text{ResNet}(a_k)$ and derive the comprehensive visual representation for the region by averaging the features of multiple images within the region. Then, a linear projection layer is utilized to project the visual feature into the representation space of region attribute, such that

$$\vec{h}_r^{img} = \text{Linear}\left(\frac{1}{m} \sum_{k=1}^m \vec{a}_k\right).$$

The contrastive loss \mathcal{L}_{img} is then used to align the visual representation with the subgraph-centric region representation, ensuring a cohesive integration of visual and attribute information.

$$\begin{aligned} \mathcal{L}_{img} = & \sum_{r \in \mathcal{R}} \left[-\log \exp \left(\frac{\vec{h}_r \cdot \vec{h}_r^{img}}{\tau} \right) \right. \\ & \left. + \log \left(\exp \left(\frac{\vec{h}_r \cdot \vec{h}_r^{img}}{\tau} \right) + \sum_{j=1}^{B-1} \exp \left(\frac{\vec{h}_r \cdot \vec{h}_j}{\tau} \right) \right) \right] \end{aligned}$$

Here, B represents batch size and τ is the temperature parameter.

A.3 Appendix of human mobility encoding

Here we give a detailed description for human mobility encoding. To learn the embeddings, we reconstruct the departure and arrival flow distribution. Let m_{ij} represent the number of trips from region r_i to region r_j . The source and destination urban flow distributions are computed as $P^{src}(r_j|r_i) = \frac{m_{ij}}{\sum_{k=1}^N m_{ik}}$ and $P^{dst}(r_i|r_j) = \frac{m_{ij}}{\sum_{k=1}^N m_{kj}}$, respectively. We then reconstruct the source and destination distributions $\hat{P}^{src}(r_j|r_i)$ and $\hat{P}^{dst}(r_i|r_j)$ using the encoded inflow and outflow features:

$$\begin{aligned} \hat{P}^{src}(r_j|r_i) &= \frac{\exp((\vec{h}_i^{src})^\top \vec{h}_j^{dst})}{\sum_k \exp((\vec{h}_i^{src})^\top \vec{h}_k^{dst})} \\ \hat{P}^{dst}(r_i|r_j) &= \frac{\exp((\vec{h}_j^{dst})^\top \vec{h}_i^{src})}{\sum_k \exp((\vec{h}_j^{dst})^\top \vec{h}_k^{src})} \end{aligned}$$

Finally, we learn the inflow and outflow embeddings by optimizing the following loss function:

$$\begin{aligned} \mathcal{L}_{flow} = & \sum_{(r_i, r_j) \in \mathcal{R} \times \mathcal{R}} -P^{src}(r_j|r_i) \log \hat{P}^{src}(r_j|r_i) \\ & - P^{dst}(r_i|r_j) \log \hat{P}^{dst}(r_i|r_j), \end{aligned}$$

which helps in accurately learning the inflow and outflow embeddings by comparing the true distributions with the reconstructed distributions.

A.4 Appendix of attribute graph kernel function

We introduce how attribute graph kernel function $K_p(\cdot, \cdot)$ works. We first define the graph kernel function $K(\cdot, \cdot)$. The graph kernel function is a P -step random walk kernel [33] to measure the similarity between graphs, which counts the number of common walks in both graphs within P steps with its calculation as follows. Given $G_1 = (V_1, E_1)$, $G_2 = (V_2, E_2)$, where V and E are the set of nodes and edges, respectively, we initially define the direct product graph G_X following the framework used in existing research [7, 33]:

$$G_X = G_1 \times G_2 = (V_X, E_X) \quad (1)$$

where $V_X = \{(v_1, v_2) : v_1 \in V_1, v_2 \in V_2\}$, $E_X = \{\{(v_1, v_2), (u_1, u_2)\} : \{v_1, u_1\} \in E_1 \wedge \{v_2, u_2\} \in E_2\}$. Following the theorem [44] that a single random walk on the direct product graph G_X is equivalent to a random walk on the two graphs G_1 , G_2 at the same time, the P -step random walk kernel is computed in the following way:

$$K(G_1, G_2) = \sum_{p=0}^P K_p(G_1, G_2) = \sum_{p=0}^P \lambda_p \sum_{i,j=1}^{|V_X|} [A_X^p]_{ij} \quad (2)$$

where A_X is the adjacency matrix of the direct product graph, λ_p is the sequence of weights and the (i, j) item of A_X^p represents the P -length common walks between the i -th and j -th nodes.

Extending the above definition to the scenario of graphs with node attributes, we use $X \in \mathbb{R}^{n \times d}$ to denote the attribute matrix of a graph with n nodes and attribute dimension d . Specifically, the node attribute matrices of G_1, G_2 are denoted by $X_1 \in \mathbb{R}^{n_1 \times d}, X_2 \in \mathbb{R}^{n_2 \times d}$. Thus, for the graph $G_X = G_1 \times G_2$, the node attribute matrix is $S = X_1 X_2^\top, S \in \mathbb{R}^{n_1 \times n_2}$, where the item (i, j) encodes the similarity between the i -th node in G_1 and the j -th node in G_2 . We flatten S to $s \in \mathbb{R}^{n_1 n_2}$ to obtain the formula for the random walk kernel:

$$K_p(G_1, G_2) = \sum_{i,j=1}^{|V_X|} s_i s_j [A_X^p]_{ij} = s^\top A_X^p s. \quad (3)$$

A.5 Appendix of dataset statistics and sources

We collect the datasets of region division, POI, urban imagery, taxi trips, road network, check-in, crime and crash for two representative cities in the United States: New York City (NYC) and Chicago (CHI). The region division is based on census tracts and the urban imagery are 256 x 256 pixels with a resolution of 4.7 meters. The detailed statistics and sources of the dataset is shown in Table 5.

Table 5: Dataset Statistics and Sources.

Data	NYC	CHI	Source
Region	180	869	Census Bureau [5]
POI	143,445	112,989	OSM [36], Safegraph [40]
Imagery	7,160	-	ArcGIS [1], UUKG [29]
Taxi trip	12,684,353	3,889,032	NYCOD [35], CHIDP [6]
Road	110,919	139,850	OSM [36]
Junction	62,437	66,065	OSM [36]
Crime	35,335	274,733	NYCOD [35], CHIDP [6]
Check-in	106,902	-	Foursquare [9, 49]
Crash	-	150,535	CHIDP [6]

A.6 Appendix of baselines description

We compare our model with representative baseline models, including graph embedding methods, knowledge graph embedding methods and state-of-the-art region embedding methods.

I. Knowledge graph embedding methods:

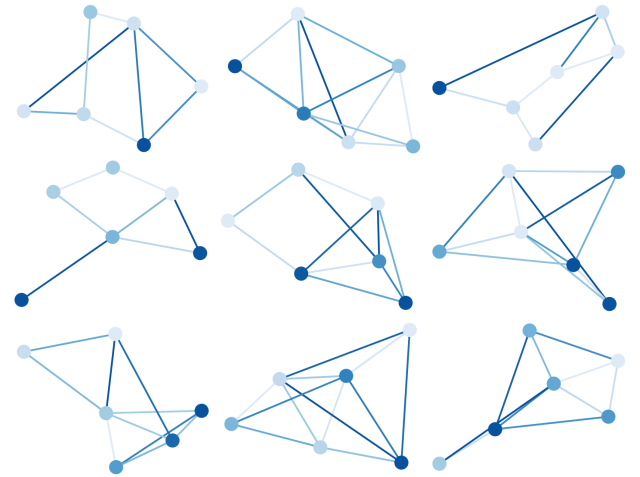
- **TransR** [25] captures the complex interactions between entities and relationships in the knowledge graph by projecting them into different spaces and learning their representation in these spaces.
- **TransR-N** method uses the embedding of the region node learned by TransR as the region representation.
- **TransR-G** method is to average the embedding of the region subgraph learned by TransR as the region representation.

II. Graph embedding methods:

- **node2vec** [12] generates a sequence of nodes by performing random walks on the graph to capture the neighborhood information of nodes, and then learns the representation of nodes using the Skip-Gram model.
- **GAE** [22] consists of an encoder and a decoder. The encoder is used to learn the representation of nodes, and the decoder tries to reconstruct the adjacency matrix from these node representation.

III. State-of-the-art urban region embedding methods:

- **MVURE** [59] constructs intra- and inter-region data multi-view based on human mobility and region attributes, and then performs multi-view fusion to learn region representation.
- **MGFN** [46] builds human mobility patterns and then learns intra- and inter-pattern relationships to obtain region representation through a multi-level cross-attention mechanism.
- **HREP** [65] designs a multi-relational heterogeneous graph of regions and used a relation-aware GCN to learn region representation, as well as a prefix prompt mechanism for downstream tasks.
- **HRE** is a part of **HREP** without prompt learning.
- **ReCP** [24] is a multi-view comparative prediction model that learns region representation by capturing the unique information of a single view as well as the consistency between two views.

**Figure 10: Visualization of additional learned prompt graphs.**

A.7 Appendix of Implementation

In our experiments, all the region embedding dimensions is set to 144. The number of HGT layer and head is 2 and 4, and the triplet margin parameter $\delta = 2$, fusion loss weight $\mu = 0.01$. We set the learning rate to 0.001 and the weight decay to 1e-6. In the task-learnable prompt module, we set the number of random walk kernel to 2 and the size of prompt graph to 6 and 8 of each layer.

We implemented our model with Pytorch 1.8, and conducted experiments on a machine equipped with a NVIDIA RTX 3090 GPU, a 64 GB RAM and a 3.50 GHz CPU.

A.8 Appendix of prompt graphs

Figure 10 displays additional learned prompt graphs, with the majority of them being circular structural features.